Acta Neuropathologica (2025) 149:26
https://doi.org/10.1007/s00401-025-02864-9

ORIGINAL PAPER

High resolution autoradiography of [^{18}F]MK-6240 and [^{18}F]Flortaucipir shows similar neurofibrillary tangle binding patterns preferentially recognizing middling neurofibrillary tangle maturity

Sujala Ghatamaneni[1] · Courtney Coleman[1] · Ian Shin[1] · Tyler Bruinsma[1] · Nancy Scott[1] · Jeyeon Lee[1,5] · Ping Fang[1] · Hoon-Ki Min[1] · Christina M. Moloney[2] · Ashley C. Wood[2] · Eleni Constantopoulos[3] · Ross R. Reichard[3] · Christopher G. Schwarz[1] · David T. Jones[4] · Jonathan Graff-Radford[4] · David S. Knopman[4] · Clifford R. Jack Jr.[1] · Ronald C. Petersen[4] · Dennis W. Dickson[2] · Melissa E. Murray[2] · Val J. Lowe[1]

Received: 18 November 2024 / Revised: 8 February 2025 / Accepted: 4 March 2025 / Published online: 14 March 2025

Abstract

Recent developments in tau positron emission tomography (PET) radiotracers have enhanced the visualization of tau aggregates in Alzheimer's disease (AD). The maturity level of neurofibrillary tangles can affect its recognition by biomarkers. Early detection of tau aggregates regarding tangle pathology is of interest in early diagnosis and comparison of tau radiotracers in this aspect is important. This study focused on head to head pathologic comparison of [^{18}F]MK-6240 and [^{18}F]Flortaucipir postmortem binding as seen on high resolution autoradiography as compared to CP-13 (early tangle maturity) and PHF-1 (middling tangle maturity) immunohistochemistry (IHC) to evaluate the tangle maturity pathology specificity of binding for tau aggregates in AD, atypical AD and non-AD tauopathies. Analyses were performed on serial 5 µm formalin-fixed paraffin-embedded human brain sections acquired from the Mayo Clinic brain bank. Visual assessment of colocalization with IHC as well as quantitative analyses were used. Evaluation of the tracers' off-target binding profiles were performed. Both tracers had similar binding properties for tau aggregates with preference to middling tangle maturity as shown by comparison to immunohistochemical distributions. Both the tracers showed strong binding to AD tau aggregates and no or minimal binding to non-AD tauopathies which corroborates with other studies.

Keywords [^{18}F]MK-6240 · [^{18}F]Flortaucipir · Tau · Alzheimer's disease · Corticobasal degeneration · Progressive supranuclear palsy · Tauopathy · Atypical Alzheimer's disease · svPPA · Frontotemporal dementia · MAPT mutation · R406W

Introduction

[^{18}F]Flortaucipir and MK 6240 are two of the most validated tau PET tracers in recent studies. Research indicates that both tracers exhibit comparable binding properties in terms of spatial distribution and severity of tau aggregates, as observed both in vivo and in vitro [1, 2, 5]. To refine diagnostic procedures and improve participant selection and treatment monitoring in trials, there is a pressing need for precise PET tracers for tau pathology across the tau pathology spectrum. Our primary objective is to assess and compare the binding properties of [^{18}F]Flortaucipir and [^{18}F]MK 6240 across different stages of tau maturity pathology.

Evidence supports the concept of neurofibrillary tangle maturation in Alzheimer's disease (AD) and three levels of maturity have been described namely,

Sujala Ghatamaneni, Courtney Coleman and Ian Shin contributed equally to this work.

✉ Val J. Lowe
vlowe@mayo.edu

1 Department of Radiology, Mayo Clinic, Rochester, MN 55905, USA

2 Department of Neuroscience, Mayo Clinic, Jacksonville, FL, USA

3 Department of Laboratory Medicine and Pathology, Mayo Clinic, Rochester, MN, USA

4 Department of Neurology, Mayo Clinic, Rochester, MN, USA

5 Department of Biomedical Engineering, College of Medicine, Hanyang University, Seoul, Republic of Korea

pretangles, mature tangles and ghost tangles [12, 13]. Tau aggregates can also vary in fibrillar tau composition, stoichiometry, hyperphosphorylation levels, and these factors can distinguish the varying tauopathies from each other [13]. The specific nature of tau pathology and their neuroanatomical distributions differ across a wide spectrum of neurodegenerative diseases. Some of these variations may also exist across the tangle lifespan in AD and in turn modulate the binding of tau PET, radiotracers. Therefore, there is a significant interest in the development of selective tau tracers to enable PET imaging of different levels of tangle maturation in AD to enhance our understanding of the natural evolution of tangles and to best select those who may be eligible for early treatment.

A key element in these considerations is that tangle maturity is an ongoing process, implying a window of opportunity to detect early maturity levels. Here we refer to early and middle tangle maturity as it relates to pathologic tangle maturity levels which has three stages of maturity that can be defined by pretangles, mature tangles and ghost tangles. To emphasize the similarity of binding properties of [^{18}F]MK-6240 and [^{18}F]Flortaucipir we have included atypical AD, frontotemporal lobar degeneration (FTLD), semantic variant primary progressive aphasia (svPPA) and microtubule associated protein tau (MAPT) mutation examples. The binding pattern of both the tracers at different stages of tangle maturity was evaluated by comparison with CP-13 and PHF-1 IHC staining. While CP-13 primarily stains pretangles and some mature tangles, PHF-1 stains a broader range, including mature tangles (middle), some pretangles (early) and some ghost tangles (advanced) [9, 12]. This variability is why PHF-1 is classified as a marker of middling tangle maturity.

Off target binding in the two radiotracers has been described as similar in a prior report [2]. The current study assessed off target binding of both the tracers in the choroid plexus and substantia nigra regions. [^{18}F]MK-6240 has shown high sensitivity and specificity comparable with [^{18}F]Flortaucipir for PHF-tau binding with favorable kinetics and fast brain delivery and washout in human study reports [17]. Similar to the previously reported [^{18}F]Flortaucipir autoradiography (ARG) study [9] and [^{18}F]MK-6240 ARG study [2], but with focus on tangle maturity pathology we undertook an in-depth head-to-head comparison of [^{18}F]Flortaucipir and [^{18}F]MK-6240 using high-resolution ARG and immunohistochemistry and used visual colocalization and image quantification assessment of the findings. Colocalization in this context refers to the spatial correspondence or overlap observed when comparing signals from ARG and IHC across aligned consecutive sections.

Methods

Tissue-sample selection

Autopsy cases with a range of neurodegenerative disorders, both with and without tau pathology, were selected from the Mayo Clinic brain bank in Jacksonville, Florida. All research was done on post-mortem samples regarded by the Mayo Clinic Institutional Review Board as exempt from the requirements of research on human participants. All brains were acquired with appropriate ethical approval, and the study was approved by the Mayo Clinic Institutional Review Board. To examine the binding specificity of the two tracers to tau pathology, neuropathologically normal individuals with no tangle or Aβ pathology, with minimal tangles and substantial Aβ pathology ("pathological aging" PA), with tangles and no Aβ pathology (primary age related tauopathy, PART), with tangle predominant dementia, and with AD were all included. Non-AD tauopathies evaluated include corticobasal degeneration (CBD), progressive supranuclear palsy (PSP), argyrophilic grains disease (AGD), and mutations linked to MAPT, including proline (P) 301 leucine (L), asparagine (N) 279 lysine (K), and arginine (R) 406 tryptophan (W). "Off-target" binding was assessed in all subjects for both tracers in the choroid plexus and substantia nigra regions.

Autoradiography

ARG of [^{18}F]MK-6240 and [^{18}F]Flortaucipir was performed on adjacent 5 µm formalin-fixed paraffin-embedded (FFPE) brain sections from the cases selected from the research brain bank. ARG and blocking experiments were performed as previously described, ARG and IHC images were adopted from our previous paper [9]. Sections were deparaffinized and incubated in 20 µCi of [^{18}F]MK-6240 or [^{18}F]Flortaucipir in 500 µL of phosphate-buffered saline (PBS) for 60 min. To demonstrate displacement ARG for non-specific binding, 30 µL of the respective reference compound (3.8 mM) was dissolved in 70 µL of ethanol (EtOH), combined with 20 µCi of [^{18}F]-labeled compound and brought up to 500 µL using PBS. This mixture was applied to adjacent sections in the same manner. Following incubation, the slides were washed in PBS for 1 min, 70% EtOH/PBS for 2 min, 30% EtOH/PBS for 1 min, and PBS for 1 min to remove the unbound tracer. Slides were air dried and then exposed to phosphor screens for 60 min. The screens were then imaged using a Typhoon FLA 7000 (GE) laser scanner.

Immunohistochemistry

Immunohistochemistry was performed on 5-µm FFPE sections using the Thermo Scientific Lab Vision Autostainer

480S that were serial to those used for ARG. Briefly, slides were deparaffinized and rehydrated using standard methods. For antigen retrieval, sections were steamed in d_2H_2O for 30 min. Sections were incubated with antibodies recognizing early tangle maturity (CP-13 [phospho-serine, 1:1,000; Peter Davies; RRID AB_2314223] or AT8 [phospho-serine 202 and threonine 205, 1:2,500; Thermo Fisher Scientific catalog # MN1020; RRID AB_223647]), or middling tangle maturity (PHF-1 [phospho-serine 396 and 404, 1:1,000; Peter Davies; RRID AB_2315150], or pS396 [phospho-serine 396, 1:1,000, Abcam catalog # ab109390, RRID:AB_10860822]). Sections were developed with a developing kit (CP-13 and PHF-1: Biocare Medical, catalog #M3M530L [mouse]; AT8 and pS396: En Vision + System-HRP Labelled Polymer Anti-mouse, DAKO Code K4001). Slides were digitally scanned at 20 × using the Aperio AT2 scanner (Leica Biosystems). Snapshots were taken using ImageScope (Leica Biosystems V12.4.3.7001).

Comparative assessment of binding

Visual comparison of autoradiographic uptake of both [^{18}F]MK-6240 and [^{18}F]Flortaucipir with immunohistochemistry was performed to assess tracer binding. Autoradiographic findings were characterized as absent (no binding above background), minimal (binding slightly above background without focal areas of intense binding), moderate (binding greater than background with a few intense focal areas much greater than the background), or strong (widespread focal and diffuse binding much greater than the background). Immunohistochemical findings were reported as absent or present. Tissue regions selected for evaluations were chosen for their specific vulnerability to tau or other pathology depending on the disorder present. Regions evaluated include posterior and anterior hippocampus, midbrain, amygdala, middle frontal cortex, subthalamic nucleus, inferior parietal cortex, superior temporal cortex, motor cortex, and basal ganglia. Regions that are spatially correlated and adjacent were used for comparison.

MATLAB Analysis

The set of images analyzed using MATLAB consisted of pairs of ARG images. These pairs were adjacent slices of brain tissue, with one slice being an [^{18}F]MK-6240 ARG and the other being an [^{18}F]Flortaucipir ARG. We selected 14 cases for quantitative analysis based on the visibility of choroid plexus on the posterior hippocampus slides. In MATLAB, each pair was co-registered to each other to create a matched image. We then evaluated the level of binding of each tracer by drawing a 1-pixel wide line through the matched images. Every pixel in the line was given a numeric value for how dark it is for the respective [^{18}F]MK-6240 and [^{18}F]Flortaucipir. As a result, we were able to graph the darkness of the individual pixels across a single line for both tracers. This allowed us to directly compare the binding of both [^{18}F]MK-6240 and [^{18}F]Flortaucipir.

We directly compared noise (area of the image outside of the brain slice), white matter, gray matter, and off-target binding. These regions of the tissue sections were visually confirmed with the pathology, and we found the specific pixel ranges of each region for every image. We then averaged the darkness of each pixel (represented by a numeric value) for the given range in the same respective region for both the [^{18}F]MK-6240 and [^{18}F]Flortaucipir images. As a result, we were able to directly compare the average binding uptake found in specific regions of the brain for both tracers.

These averages were then standardized and normalized across all images for direct comparison and statistical analysis. By default, MATLAB represents darker areas as being closer to zero. Because the darker areas of ARG represented binding uptake, so we standardized the data by subtracting the average noise value across all images from white matter, gray matter, and off-target binding areas respectively, and took the absolute value of the difference. The standardized data were normalized by dividing the standardized white matter value for each image.

Results

The participant characteristics in this study are summarized in Table 1. A total of 38 participants were examined. Examples from 18 of these participants are shown in the figures described below. The participants included a spectrum from normal to AD, including mild cognitive impairment (MCI) and atypical AD. To confirm specificity atypical AD, svPPA pathologically AD confirmed, case is included. Within the confirmed 3R/4R tau isoforms participants, diffuse Lewy body disease (DLBD), PART, and tangle predominant dementia participants were included. 4R tau (CBD, PSP, AGD) cases were included. Participants with N279K (4R), P301L (4R), and R406W MAPT mutations (3R + 4R) were included as well. Finally, participants with off-target binding sites of the choroid plexus and substantia nigra were integrated.

Atypical AD subject

Figure 1 depicts a neuropathologically diagnosed AD (Braak stage VI and Thal stage 5) [^{18}F]MK-6240 shows strong binding (Fig. 1A, G) in tangle-burdened regions by CP-13 and PHF-1 immunohistochemistry staining (Fig. 1E, F, K, L; Q shows zoomed immunohistochemical staining to show tangles) both in the posterior hippocampus (top row) and

Table 1 Participant characteristics of tauopathies

Case	Clinical diagnosis	Neuropathologic diagnosis	TDP type	Tau isoform	Braak	Thal	Age	Sex
1	Normal	Normal	0	–	0	0	81	F
2	Normal	Normal	0	–	0	0	68	M
3	Normal	Normal	0	–	0	0	65	M
4	MCI	PA	0	3R + 4R	III	2	88	F
5	svPPA	AD (HpSp)/DLBD	0	3R + 4R	VI	5	60	M
6	Normal	PART	0	3R + 4R	III–IV	0	89	F
7	MCI	Tangle predominant dementia	0	3R + 4R	III	0	81	F
8	AD	Tangle predominant dementia	0	3R + 4R	IV	0	82	M
9	PSP	PSP	0	4R	II–III	1	68	F
10	PSP	PSP	0	4R	I	0	65	M
11	Normal	AGD	0	4R	III	1	91	M
12	PPND	FTDP-17 (MAPT N279K)	0	4R	0	0	49	M
13	FTD	FTDP-17 (MAPT P301L)	0	4R	0	0	53	M
14	FTD	FTDP-17 (MAPT R406W)	0	3R + 4R	5	0	66	F
15	svPPA	AD	0	3R + 4R	VI	5	77	M
16	CBD	NBIA	0	3R + 4R	V	0	51	M
17	MCI	PART-NFT	0	3R + 4R	V	V	87	F
18	AD	Tangle predominant	0	3R + 4R	IV	0	83	F

De-identified case numbers are present throughout the text within figures. Braak refers to the neurofibrillary tangle stage, and Thal refers to the amyloid phase

MCI Mild cognitive impairment, *PA* pathological aging, *svPPA* semantic variant Primary Progressive Aphasia, *AD* Alzheimer's disease, *DLBD* diffuse Lewy body disease, *PART* primary age-related tauopathy, *AGD* argyrophilic grains disease, *PiD* Pick's disease, *CBD* corticobasal degeneration, *PSP* progressive supranuclear palsy, *PPND* Pallido-ponto-nigral degenereation, *FTDP-17* frontotemporal dementia, and parkinsonism linked to chromosome 17, *3R* 3 repeat tau, *4R* 4 repeat tau, *F* female, and *M* male. De-identified case numbers are present throughout the text within figures

HpSp hippocampal sparing, *NBIA* neurodegeneration with brain iron accumulation

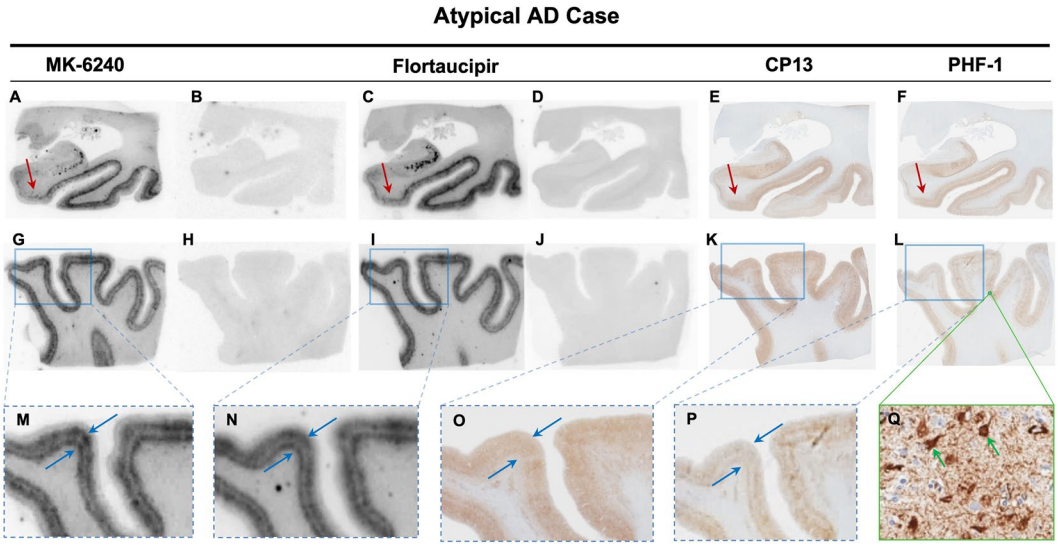

Fig. 1 Atypical Alzheimer's disease (AD) case. Matching autoradiography (ARG) and immunohistochemical (IHC) in Atypical AD of Braak VI and Thal 5 stages (Participant 15). Clinical diagnosis of semantic variant primary progressive aphasia and confirmed AD by neuropathology. First row showing posterior hippocampal regions (**A**–**F**) (Red arrow indicating parahippocampal gyrus), second row showing parietal regions (**G**–**L**), and third row showing 2.5 × magnification of the parietal regions (M-P) (Blue arrow showing the cortical double layers, internal granular and external granular layer). [^{18}F]MK-6240 (**A**, **G**, **M**) and [.^{18}F] Flortaucipir (**C**, **I**, **N**) ARG with associated blocking slides (**B**, **D**, **H**, **J**). CP-13 IHC (**E**, **K**, **O**) representing early pretangles and PHF-1 IHC (F, L, P) representing mature tangles. Q showing 20 × magnification of PHF-1 IHC (Green arrow showing mature tangles)

parietal cortex (bottom row). The pattern of early tangle maturity confirmed by CP-13 (Fig. 1F, L) and middle tangle maturity seen with PHF-1 (Fig. 1E, K). Red arrows highlight the parahippocampal gyrus (top row), showing strong ARG signals. This binding was confirmed with the use of blocked adjacent sections to show the selectivity of the tracer binding signal (Fig. 1B, H). The [^{18}F]MK-6240 binding patterns showed good consistency with [^{18}F]Flortaucipir in an adjacent section (Fig. 1C,I; block confirmation of [^{18}F] Flortaucipir in Fig. 1D,J). The expanded view (Fig. 1 M, N, O, P) confirms the cortical double layers, internal granular and external granular layer (indicated by blue arrows) seen with ARG in both [^{18}F]MK-6240 and [^{18}F]Flortaucipir, which corresponded best with PHF-1 patterns as compared to CP-13 indicating that both the tracers have middle tangle maturity preference.

Direct quantitative comparison of [^{18}F]Flortaucipir and [^{18}F]MK-6240

In Fig. 2, a sample pair of correlative ARG images and immunohistochemical findings are shown to demonstrate our quantitative data collection process. Colocalization with tau IHC was similar in both [^{18}F]MK-6240 and [^{18}F] Flortaucipir. Choroid plexus off-target binding was often present in both tracers. [^{18}F]Flortaucipir showed higher (mean, 31%) binding in the off-target area (red arrows) and lower (mean, 14%) binding in the gray matter area (blue arrows). In 14 cases with posterior hippocampus tissue, [^{18}F]MK-6240 had higher gray matter uptake compared to [^{18}F]Flortaucipir in ten out of fourteen cases and off target [18F]Flortaucipir had higher binding in 9 out of 14 cases(Fig. 2D). In Fig. 6, PHF-1 immunoreactivity was seen in the hippocampal, parahippocampal, fusiform and inferior temporal regions (Fig. 6C, F, I) with subtle variations in [^{18}F]MK-6240 vs [^{18}F]Flortaucipir binding colocalization to IHC (Fig. D, E, G and H).

Early tangle maturity accumulation subjects

In Fig. 3, AD and non-AD neurodegenerative disease participants with early tau accumulation are shown with CP-13 and PHF-1 immunohistochemistry. A clinically normal participant confirmed by autopsy showed no tau specific binding in any regions with either of the tracers with some mild, similar, off-target lateral geniculate nucleus binding in both served as positive control (Fig. 3A, B). There was no tau staining by immunohistochemistry with either CP-13 or PHF-1 (Fig. 3C, D). A participant clinically diagnosed with MCI (PA) showed tau pathology with CP-13 immunohistochemistry in the CA1 (cornu ammonis) region of the hippocampus (red arrows) and PHF-1 (Fig. 3G, H).

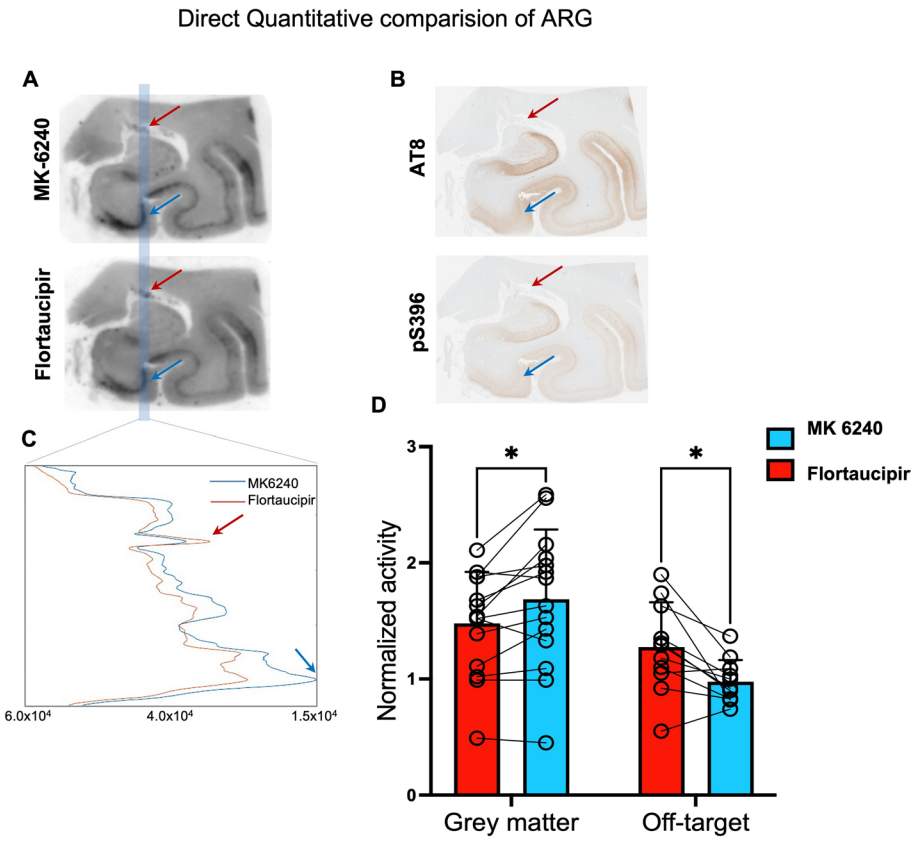

Fig. 2 Direct comparison of [^{18}F]MK-6240 and [^{18}F] Flortaucipir ARG ($n = 10$). The ARG was conducted simultaneously using the two radioisotopes in adjacent slides. **A** Sample pair of correlative autoradiography (ARG) and **B** immunohistochemical findings. Blue lines indicate the single line of pixels to derive Graph (**C**). **C** Graph shows the blue line representing [^{18}F] MK-6240 in blue line and [.^{18}F] Flortaucipir in red line. Red arrows indicate off-target binding of Choroid Plexus on the ARG images, graph and shown in the IHC slides (**A**, **B**, **C**). Blue arrows indicate peak gray matter binding area in the ARG, graph and in the IHC slides (**A**, **B**, **C**). Summary comparison of gray matter binding and off-target binding between the two tracers (**D**)

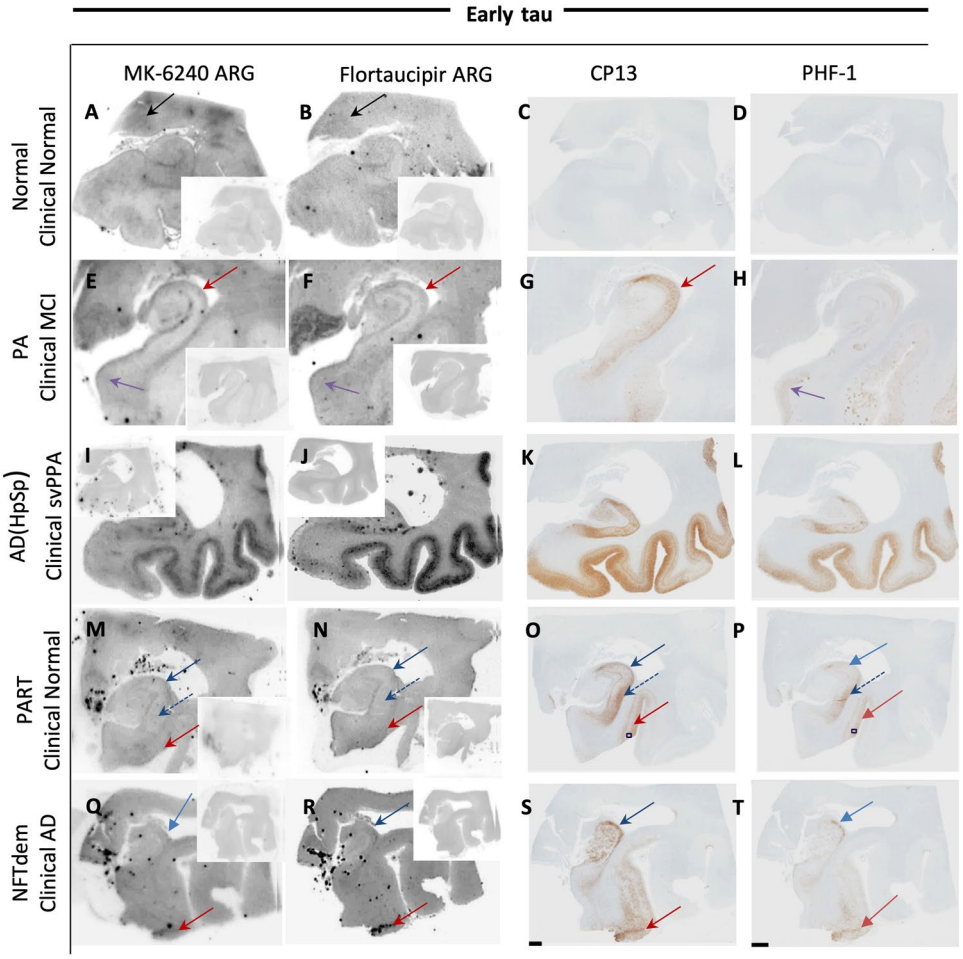

Fig. 3 Correlative [^{18}F]MK-6240 and [^{18}F] Flortaucipir autoradiography (ARG) and immunohistochemistry (IHC) assessing early tau accumulation. **A**–**D** participant 2 –Clinically normal confirmed by autopsy showed no specific tau binding with some mild, similar, off target binding (black arrows). **A**, **B** no tau staining either with IHC sections CP-13 and PHF-1 **C**, **D**. **E**–**H** participant 4—pathological aging clinically diagnosed with MCI showed tau pathology with immunohistochemistry CP-13 in the CA1 (cornu ammonis) region of the hippocampus (red arrow) (H) and PHF-1 in the parahippocampal gyrus (purple arrow) **G**. Neither tracer showed convincing co localizing binding in the same regions (red and blue arrows) **E**, **F**. **I**–**L**, participant 5– Hippocampal sparing (HpSp) Alzheimer's disease (AD) included to show AD-type tau binding., **M**–**P** participant 6 – Primary age-related tauopathy (PART) in clinically normal showed tau pathology in the CA1 (blue arrows) subiculum (dashed blue arrows) of the hippocampus and the transentorhinal cortex (red arrows) **O**, **P**, again neither tracer showed detectable colocalizing binding in these regions **M**, **N**. **Q**–**T**, participant 8 – Neurofibrillary tangle predominant dementia showed tau pathology in the CA1 region hippocampus (blue arrow), transentorhinal cortex (red arrow) **S**, **T**. [^{18}F] Flortaucipir showed minor evidence of binding (red & blue arrows), while [^{18}F]MK-6240 had more limited visible binding (red & blue arrows). Early tau accumulations participants had more tau demonstrated with CP-13 than PHF-1. Blocking slides shown in the ARG insets

Neither tracer showed convincing colocalizing binding in the same regions (Fig. 3E, F). A hippocampal sparing AD participant is included here (Fig. 3I–L) to show AD-type tau binding. A PART participant clinically diagnosed as normal showed tau pathology in the CA1 (blue arrows) and subiculum (dashed blue arrows) of the hippocampus and the parahippocampus gyrus (red arrows) (Fig. 3O, P), but neither tracer showed detectable colocalizing binding in these regions (Fig. 3M, N). A tangle predominant dementia participant showed tau pathology in the CA1 region of the hippocampus (blue arrows), as well as the parahippocampal gyrus (red arrows) (Fig. 3S, T), confirmed with CP-13 immunohistochemistry (Fig. 3S). [^{18}F]Flortaucipir showed minor evidence of binding (Fig. 3R; blocking confirmation in inset), while [^{18}F]MK-6240 had more limited visible binding (Fig. 3 Q). Generally, early tangle maturity tau accumulation participants had more tau demonstrated with CP-13 than PHF-1 and both the tracers binding are well correlated with the PHF-1 staining suggesting the preference for middling tangle level and minimal to early tangles.

4R tauopathies

Figure 4 presents CBD, PSP, and AGD participantsPHF-1 immunoreactivity was observed in the subthalamic nucleus in CBD (Fig. 4C), and minimal binding was observed using both [^{18}F]Flortaucipir and [^{18}F]MK-6240, with [^{18}F] Flortaucipir showing slightly more binding (red arrows, Fig. 4A, B). In the motor cortex in CBD, minimal tau activity was seen (Fig. 4F) with no binding present from either tracer (Fig. 4D, E). The frontal cortex in CBD showed white matter PHF-1 immunoreactivity (Fig. 4I) that was minimally detected by both tracers (red arrows, Fig. 4G, H). In the frontal cortex of PSP, a small amount of immunopositivity was observed with PHF-1 immunohistochemistry shown in red arrow and blue arrow indicate likely ARTAG (Fig. 4L) which was detected by both the tracers (blue arrows, Fig. 4J, K) with very minimal tau binding from either tracer shown in red arrows (J, K). In the motor cortex of the PSP case, minimal tau activity was seen (red arrows, Fig. 4O), with very minimal detectable binding from either tracer (Fig. 4M, N). The subthalamic nucleus of PSP showed PHF-1 immunopositivity (red arrows, Fig. 4R) with minimal detectable binding from either tracer again (Fig. 4P, Q). In the posterior hippocampus of a case of AGD, there appeared to be PHF-1 immunoreactivity (Fig. 4U); however, binding is not observed when using either tracer (Fig. 4S, T). The temporal cortex of the same participant did not show any PHF-1 immunoreactivity (Fig. 4 X), and there was no signal from either tracer (Fig. 4V, W). Radiotracer clumping artifact and radiotracer uptake about blood vessels as dots of focal tracer signal are seen on several of the images and is non-specific.

MAPT mutation participants

Figure 5 shows MAPT mutation participants, including N279K, P301L, and R406W. PHF-1 showed immunoreactivity in the white matter of the temporal cortex of mutation N279K (Fig. 5C) with the similar binding present by both tracers (Fig. 5A, B). Some PHF-1 immunoreactivity in the temporal cortex was seen in the granular layers of mutation P301L (Fig. 5F), and minimal correlative binding to this area was observed

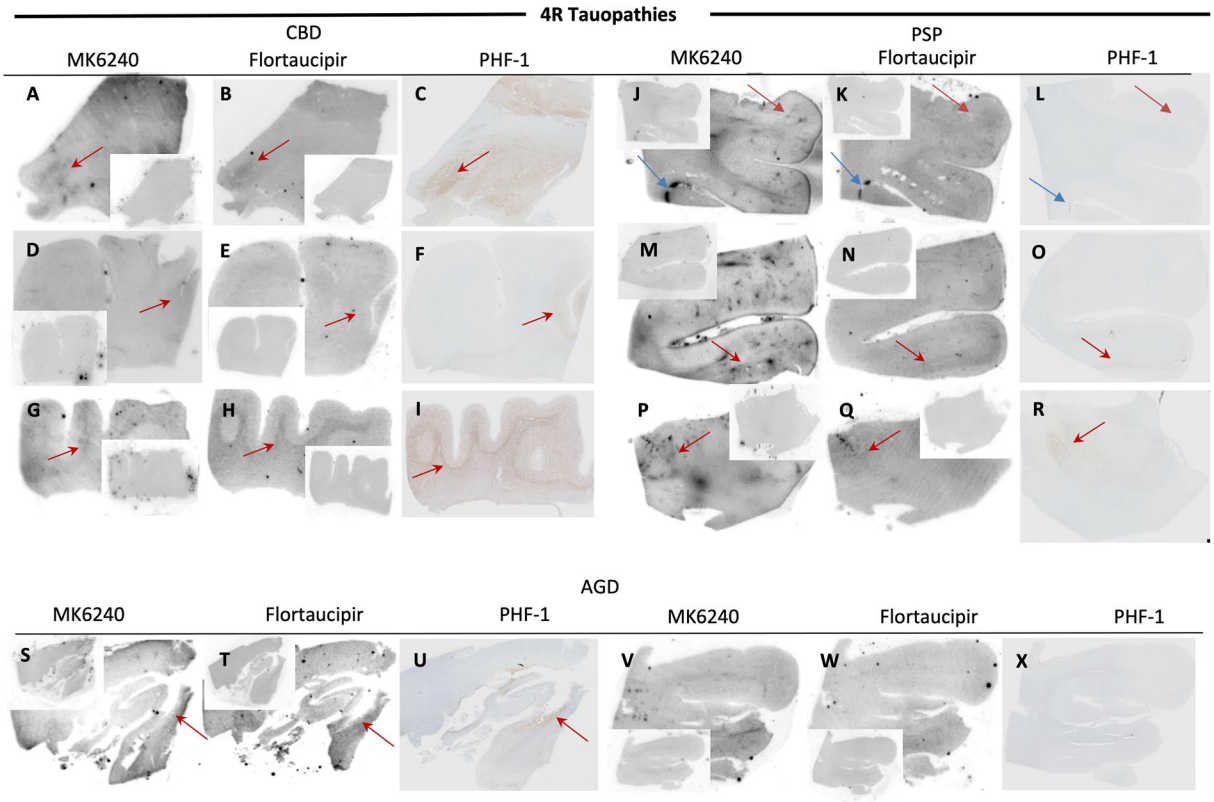

Fig. 4 Correlative autoradiography (ARG) and immunohistochemical (IHC) findings for assessment of 4R Tau (CBD, PSP, and AGD) binding. **A-I** participant 16- CBD, **J–R** participant 10—PSP, **S–X** participant 11—AGD. Shown from left to right [^{18}F]MK-6240 ARG, [^{18}F]Flortaucipir ARG (blocking shown in the ARG insets), and PHF-1 IHC slides, subthalamic nucleus **A–C** and **P–R**, motor cortex **D–F** and **M–O**, frontal cortex **G–I** and **J–L**, post hippocampus **S–U**, temporal cortex **V–X**. Red arrows indicate absent or minimal binding in both tracers

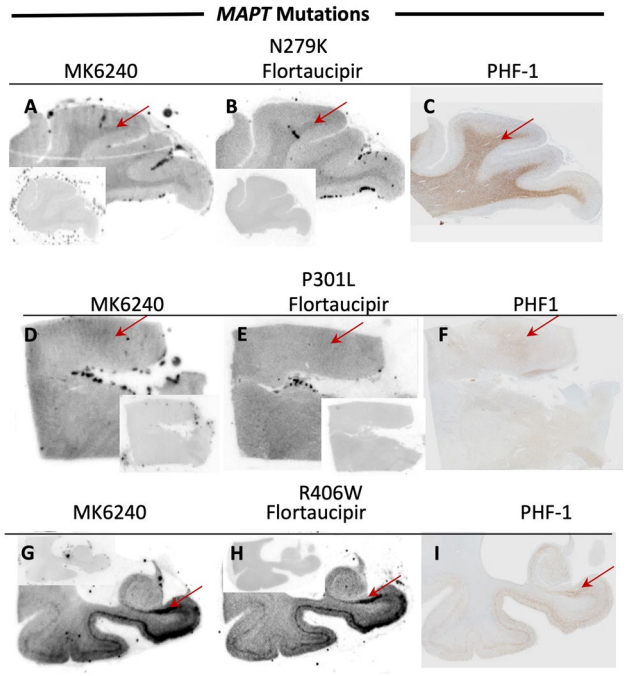

Fig. 5 Correlative autoradiography (ARG) and immunohistochemical (IHC) findings for assessment of MAPT mutation (N279K, P301L, and R406W) tau binding. **A–C** Case 12—FTDP-17 (MAPT N279K), **D–F** Case 13—FTDP-17 (MAPT P301L), **G–I** Case 14—FTDP-17 (MAPT R406W). Shown from left to right MK-6240 ARG, Flortaucipir ARG (blocking shown in the ARG insets), and PHF-1 IHC in the temporal cortex (**A–F**, and anterior hippocampus **G–I**. **A–C** red arrows indicates immunoactivity in the white matter **C** with the similar binding present by both the tracers **A**, **B**. **D–F** red arrows indicate some immunoactivity seen in the granular layers **F** and minimal correlative binding to this area observed with both the tracers **D**, **E**. **G–I** red arrows indicate immunoreactivity in **I** that correlated to strong binding of both tracers in several regions in a similar distribution **G**, **H**

with both tracers.(Fig. 5D,E) Mutation R406W showed immunoreactivity in the anterior hippocampus (Fig. 5I) that correlated to strong binding of both tracers in this and several regions in a similar distribution (red arrows, Fig. 5G, H).

Off-target binding

In Fig. 6, [^{18}F]MK-6240 and [^{18}F]Flortaucipir both showed off-target binding in the choroid plexus and substantia nigra, although with different intensities. Tracer binding was prevalent in these off-target regions without corresponding reactivity on PHF-1 (represented with orange arrows). In some cases [^{18}F]MK-6240 showed greater off-target binding in the choroid plexus (Fig. 6D), while in others [^{18}F]Flortaucipir binding was greater. Overall, [^{18}F]Flortaucipir had greater off-target binding (31%) (Fig. 6B and H A and Fig. 2D). In the substantia nigra, PHF-1 immunoreactivity was very minimal (Fig. 6L, O, R). While both tracers showed significant off-target binding, [^{18}F]MK-6240 generally showed less off-target binding (Fig. 6J, M, P) compared to that of [^{18}F] Flortaucipir in the substantia nigra (Fig. 6 K, N, Q).

Discussion

This study compared [^{18}F]MK-6240 and [^{18}F]Flortaucipir with IHC CP-13 and PHF-1 stains to evaluate and compare the binding to the tangle maturity levels in AD and non-AD cases. Both tracers had binding that was more closely related to PHF-1 than CP-13, suggesting that both [^{18}F]MK-6240 and [^{18}F]Flortaucipir recognize a middling tangle maturity level. Both tracers show no high binding in non-AD tauopathies.

Neurofibrillary tangles maturity levels differ in their morphology, tau isoform predilection and post translational modifications [12, 13]. Being able to detect tangles at different tangle maturity levels could be very helpful for understanding disease progression and for treatment assessment. These data show that these differences of tangle maturity levels may have influence on tau-PET signal. For instance, in cases of PART, which can vary from mild pretangles in the hippocampus to advanced stages characterized by ghost tangles [4], Radiotracer binding was not clearly detected in PART in this work. Minimal binding was previously observed in regions with abundant ghost tangles [9]. Together these data suggest that the tracer binding pattern is more sensitive to middle or mature tangle pathology. There is a need for more research to determine the complete range of tau-PET tracer profiles in both tau severity and tangle maturity.

More recently, other tau tracers have been developed in the hope of resolving some of the challenges found with the first-generation tracers. Ideally, new tau PET tracers can be developed to bind to not only AD-typical 3R/4R tau isoforms but other isoforms (e.g. 3R and 4R) as well. More recent tracers include [^{18}F]PM-PBB3, [^{18}F]GTP1, [^{18}F] PI-2620 and [^{18}F]MK-6240. Prior autoradiographic assessment of [^{18}F]MK-6240 reported similar binding patterns to that of [^{18}F]Flortaucipir [2]. This study showed a similar preference to middling stage tangle maturity level in both the tracers. Some human PET studies of [^{18}F] MK-6240 report a wide dynamic range with minimal off-target binding [3, 8]. In our study, the overall data differs somewhat with these in vivo reports by demonstrating that [^{18}F]MK 6240 off-target binding is common but less than [^{18}F]Flortaucipir in choroid plexus and substantia nigra. We showed that [^{18}F]MK-6240 and [^{18}F]Flortaucipir have similar features in detecting middling tangle maturity

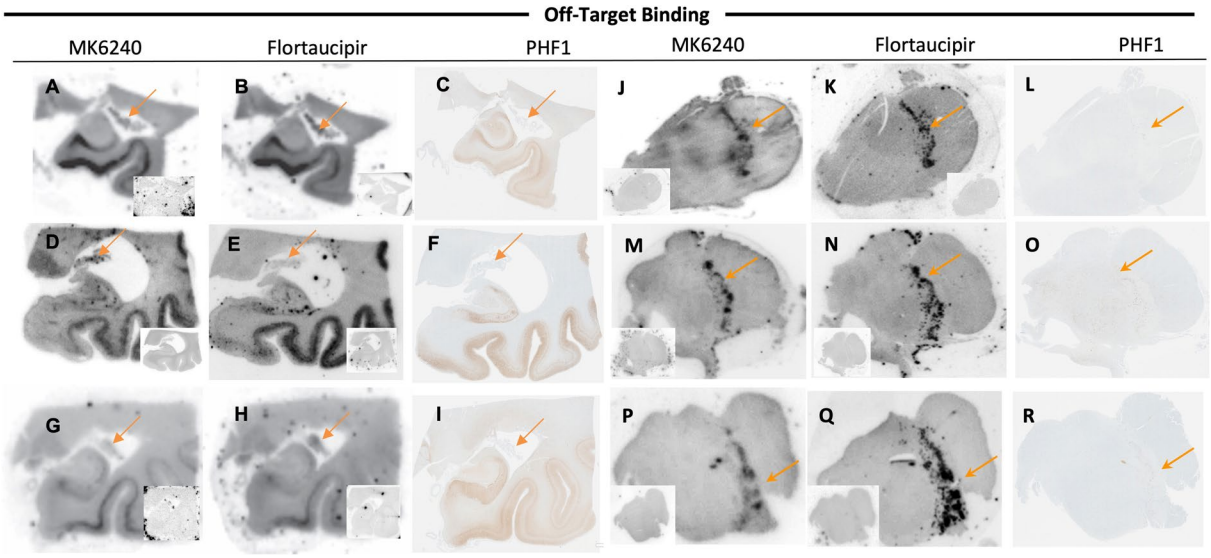

Fig. 6 Correlative autoradiography (ARG) and immunohistochemical (IHC) findings for assessment of off-target binding sites. **A–C** Participant 17—choroid plexus, **D–F** Participant 5—choroid plexus, **G–I** Participant 18—choroid plexus, **J–L** Participant 3—substantia nigra (midbrain), **M–O** Participant 10—substantia nigra (midbrain), **P–R** Participant 1—substantia nigra (midbrain). Shown from left to right MK-6240 ARG, Flortaucipir ARG, and PHF-1 IHC in the posterior hippocampus **A–I**, midbrain **J–R**, and amygdala **S–U**. A-I orange arrows indicate choroid plexus and PHF-1 immunoreactivity seen in the hippocampal region and orange arrows indicate choroid plexus **C**, **F**, **I**, [^{18}F]MK-6240 showed off-target binding in the choroid plexus **D**, while [^{18}F] Flortaucipir appeared to have binding present **B** and **H**. J-R orange arrows indicate in the substantia nigra PHF-1 immunoactivity was very minimal **L**, **Q**, **R**, while both tracers showed significant off target binding, [^{18}F]MK-6240 showed less off-target binding **J**, **M**, **P** compared to [^{18}F] Flortaucipir **K**, **N**, **Q**

pathology. Prior reports suggested [^{18}F]MK-6240 blocks [^{18}F]Flortaucipir ARG binding, implying a similar binding site between the two compounds. In silico analysis have shown that [^{18}F]Flortaucipir has at least two identical binding sites on tau fibrils with [^{18}F]MK-6240 [11]. It has also been suggested that [^{18}F]Flortaucipir can change the conformation or the accessibility of the [^{18}F]MK-6240 specific binding site on the tau fibril, preventing the binding of [^{18}F]MK-6240 to its target site [11]. Our high-resolution autoradiographic further shows the internal granular and external granular layers are seen with PHF-1 in both [^{18}F]MK-6240 and [^{18}F]Flortaucipir. While the major distribution pattern correlates with PHF-1, which represents middle tangle pathology, our results showed reduced colocalization with the CP-13 pattern, which assesses primarily early tangle pathology.

Early tangle maturity identification and longitudinal tracking and quantification of tau tangles in participants with AD could be crucial for understanding the natural history of AD, as well as for developing clinical trials, anti-tau therapies, and treatment response assessment. In vivo Braak stages using tau-PET imaging may help stratify living participants based on patterns of tau deposition. However, prior studies have shown that tau-PET tracers have low sensitivity for detecting early Braak stage tau deposition. While some human studies have shown [^{18}F]MK-6240 based standardized uptake value ratio (SUVR) values may stratify individuals with pathologic tau deposition from early Braak regions (stage I-II) in asymptomatic participants [14, 15], in this ARG study, both [^{18}F]MK-6240 and [^{18}F]Flortaucipir struggled at detecting early Braak stage tau deposition. While this could be seen as conflicting, our data may still be assessing earlier neurofibrillary tangle disease. In Fig. 3, the Hippocampal sparing AD case demonstrates additional variability as [^{18}F]MK 6240 showed less intense binding compared to [^{18}F]Flortaucipir. The nature of these findings will require further evaluations. In addition, the influence of off-target signal from such things as meninges are not contributing to these ARG findings as they could be in human investigations. Future work to compare both [^{18}F] MK-6240 and [^{18}F]Flortaucipir in the same participants with early Braak stage findings will be helpful in this regard.

Frontotemporal dementia (FTD) comprises a heterogenous group of proteinopathies, including but not limited to TDP-43 [10]. Microtubule associated protein tau (MAPT) mutations can lead to tauopathy and FTD. In our present study both [^{18}F]MK-6240 and [^{18}F]Flortaucipir showed moderately strong binding pattern to R406W MAPT mutation which correlates with in vivo studies on [^{18}F] MK-6240 [7]. Recent studies showed notably higher SUVR values being obtained in the participant with an R406W MAPT mutation compared to milder binding in participants with a P301L MAPT mutation [7]. The binding of [^{18}F] MK-6240 and [^{18}F]Flortaucipir was absent or minimal in

non-AD tauopathies and MAPT mutations (N279K and P301L) [1, 2].

Off-target binding of [^{18}F]Flortaucipir and [^{18}F]MK-6240 was variable in the choroid plexus and substantial nigra and generally modestly lower in [^{18}F]MK 6240. Previous studies suggested that off-target binding of [^{18}F]Flortaucipir (first generation tau-PET tracer) may be due to its affinity for monoamine oxidase B (MAO-B) and neuromelanin[6, 16]. However recent in vitro studies ruled out the binding of [^{18}F] MK-6240 and [^{18}F]Flortaucipir tracers to MAO-A and B [1].

It is important to note that although in our study [^{18}F] MK-6240 and [^{18}F]Flortaucipir have shown similar visual distribution patterns on post-mortem sections, in vivo studies have shown higher affinity of [^{18}F]MK-6240 for PHF-tau compared to that of [^{18}F] Flortaucipir with a nearly twofold higher dynamic range [5]. Various other factors such as radiotracer metabolism, blood brain barrier permeability, nonspecific binding, and rates of plasma and reference region clearance may influence in vivo imaging assessment and qualitative measurements of these two radiotracers [3, 18].

In conclusion, the emergence and validation of these new tau PET tracers have opened new opportunities for the development of more accurate diagnostic and management tools for AD. In our study on post-mortem sections, [^{18}F] MK-6240 and [^{18}F]Flortaucipir showed similar binding profiles with preference to middle tangle maturity levels.

Acknowledgements We would like to thank Avid Radiopharmaceuticals, Inc., for their support in supplying [18F] Flortaucipir precursor, chemistry production advice. We would like to thank Merck Research Laboratories (Rahway, NJ or West Point, PA) for their support for [18F]MK-6240. We are grateful to Seokbeen Lim, PhD, Virginia Phillips, Monica Castanedes-Casey, Ariston Librero, Jo Landino, Jessica Tranovich, Ashley Wood, and the Cytometry and Imaging Lab for histologic and imaging support.

Author contributions All authors contributed equally.

Declarations

Competing interests The authors declare no competing interests.

References

1. Aguero C, Dhaynaut M, Amaral AC, Moon SH, Neelamegam R, Scapellato M et al (2024) Head-to-head comparison of [(18)F]-Flortaucipir, [(18)F]-MK-6240 and [(18)F]-PI-2620 postmortem binding across the spectrum of neurodegenerative diseases. Acta Neuropathol 147:25. https://doi.org/10.1007/s00401-023-02672-z
2. Aguero C, Dhaynaut M, Normandin MD, Amaral AC, Guehl NJ, Neelamegam R et al (2019) Autoradiography validation of novel tau PET tracer [F-18]-MK-6240 on human postmortem brain tissue. Acta Neuropathol Commun 7:37. https://doi.org/10.1186/s40478-019-0686-6
3. Betthauser TJ, Cody KA, Zammit MD, Murali D, Converse AK, Barnhart TE et al (2019) In Vivo Characterization and Quantification of Neurofibrillary Tau PET Radioligand (18)F-MK-6240 in Humans from Alzheimer Disease Dementia to Young Controls. J Nucl Med 60:93–99. https://doi.org/10.2967/jnumed.118.209650
4. Crary JF, Trojanowski JQ, Schneider JA, Abisambra JF, Abner EL, Alafuzoff I et al (2014) Primary age-related tauopathy (PART): a common pathology associated with human aging. Acta Neuropathol 128:755–766. https://doi.org/10.1007/s00401-014-1349-0
5. Gogola A, Minhas DS, Villemagne VL, Cohen AD, Mountz JM, Pascoal TA et al (2022) Direct Comparison of the Tau PET Tracers (18)F-Flortaucipir and (18)F-MK-6240 in Human Subjects. J Nucl Med 63:108–116. https://doi.org/10.2967/jnumed.120.254961
6. Lemoine L, Saint-Aubert L, Nennesmo I, Gillberg PG, Nordberg A (2017) Cortical laminar tau deposits and activated astrocytes in Alzheimer's disease visualised by (3)H-THK5117 and (3)H-deprenyl autoradiography. Sci Rep 7:45496. https://doi.org/10.1038/srep45496
7. Levy JP, Bezgin G, Savard M, Pascoal TA, Finger E, Laforce R et al (2022) 18F-MK-6240 tau-PET in genetic frontotemporal dementia. Brain 145:1763–1772. https://doi.org/10.1093/brain/awab392
8. Lohith TG, Bennacef I, Vandenberghe R, Vandenbulcke M, Salinas CA, Declercq R et al (2019) Brain Imaging of Alzheimer Dementia Patients and Elderly Controls with (18)F-MK-6240, a PET Tracer Targeting Neurofibrillary Tangles. J Nucl Med 60:107–114. https://doi.org/10.2967/jnumed.118.208215
9. Lowe VJ, Curran G, Fang P, Liesinger AM, Josephs KA, Parisi JE et al (2016) An autoradiographic evaluation of AV-1451 Tau PET in dementia. Acta Neuropathol Commun 4:58. https://doi.org/10.1186/s40478-016-0315-6
10. Mackenzie IR, Neumann M, Bigio EH, Cairns NJ, Alafuzoff I, Kril J et al (2010) Nomenclature and nosology for neuropathologic subtypes of frontotemporal lobar degeneration: an update. Acta Neuropathol 119:1–4. https://doi.org/10.1007/s00401-009-0612-2
11. Malarte ML, Nordberg A, Lemoine L (2021) Characterization of MK6240, a tau PET tracer, in autopsy brain tissue from Alzheimer's disease cases. Eur J Nucl Med Mol Imaging 48:1093–1102. https://doi.org/10.1007/s00259-020-05035-y
12. Moloney CM, Lowe VJ, Murray ME (2021) Visualization of neurofibrillary tangle maturity in Alzheimer's disease: A clinicopathologic perspective for biomarker research. Alzheimers Dement 17:1554–1574. https://doi.org/10.1002/alz.12321
13. Murray ME, Kouri N, Lin WL, Jack CR Jr, Dickson DW, Vemuri P (2014) Clinicopathologic assessment and imaging of tauopathies in neurodegenerative dementias. Alzheimers Res Ther 6:1. https://doi.org/10.1186/alzrt231
14. Pascoal TA, Benedet AL, Tudorascu DL, Therriault J, Mathotaarachchi S, Savard M et al (2021) Longitudinal 18F-MK-6240 tau tangles accumulation follows Braak stages. Brain 144:3517–3528. https://doi.org/10.1093/brain/awab248
15. Pascoal TA, Therriault J, Benedet AL, Savard M, Lussier FZ, Chamoun M et al (2020) 18F-MK-6240 PET for early and late

detection of neurofibrillary tangles. Brain 143:2818–2830. https://doi.org/10.1093/brain/awaa180
16. Vermeiren C, Motte P, Viot D, Mairet-Coello G, Courade JP, Citron M et al (2018) The tau positron-emission tomography tracer AV-1451 binds with similar affinities to tau fibrils and monoamine oxidases. Mov Disord 33:273–281. https://doi.org/10.1002/mds.27271
17. Walji AM, Hostetler ED, Selnick H, Zeng Z, Miller P, Bennacef I et al (2016) Discovery of 6-(Fluoro-(18)F)-3-(1H-pyrrolo[2,3-c]pyridin-1-yl)isoquinolin-5-amine ([(18)F]-MK-6240): A Positron Emission Tomography (PET) Imaging Agent for Quantification of Neurofibrillary Tangles (NFTs). J Med Chem 59:4778–4789. https://doi.org/10.1021/acs.jmedchem.6b00166
18. Wooten DW, Guehl NJ, Verwer EE, Shoup TM, Yokell DL, Zubcevik N et al (2017) Pharmacokinetic Evaluation of the Tau PET Radiotracer (18)F-T807 ((18)F-AV-1451) in Human Subjects. J Nucl Med 58:484–491. https://doi.org/10.2967/jnumed.115.170910